Materials Research Bulletin 107 (2018) 492–497

Contents lists available at ScienceDirect

Materials Research Bulletin

journal homepage: www.elsevier.com/locate/matresbu

The synthesis of CuO and NiO nanoparticles by facile thermal decomposition of metal-Schiff base complexes and an examination of their electric, thermoelectric and magnetic Properties

E.M.M. Ibrahim[a,*], Laila H. Abdel-Rahman[b], Ahmed M. Abu-Dief[b], A. Elshafaie[a], Samar Kamel Hamdan[b], A.M. Ahmed[a]

[a] Physics Department, Faculty of Science, Sohag University, Sohag 82524, Egypt
[b] Chemistry Department, Faculty of Science, Sohag University, Sohag 82524, Egypt

ARTICLE INFO

Keywords:
CuO
NiO
magnetic
nanoparticles
Schiff base complexes
thermoelectric

ABSTRACT

In this study, CuO and NiO NPs have been synthesized by facile thermal decomposition of Schiff base complexes and their physical properties have been examined. The synthesized CuO and NiO NPs are crystallized in polycrystalline monoclinic and cubic structures with average particle size 17 ± 0.4 and 62 ± 1 nm, respectively. The electrical conductivity measurements confirm that the conduction in the CuO NPs is a band-to-band type while the conduction in the NiO NPs is governed by the large polaron conduction mechanism. The thermoelectric measurements confirm that the CuO and NiO NPs are P-type degenerate semiconductors with room temperature Seebeck coefficients equal to 89.9 and 12.1 mV/K, respectively. The magnetic measurements exhibit that the NPs have weak ferromagnetic ordering and antiferromagnetic to paramagnetic transition with high dipolar interaction.

1. Introduction

Due to their extraordinary properties, metal oxide nanostructures are promising candidates for applications in various fields such as optoelectronics, optics, catalysts, sensors and electronics [1–15]. Among many metal oxides, CuO is a narrow band gap (1.2 eV) p-type semiconductor and thus it has received much attention for applications in optoelectronics, catalysis, semiconductors, batteries, gas sensors, biosensors and field transistors [4,5]. Also, NiO is a p-type semiconductor with relatively wide band gap (3.6 eV) and it has great potential applications such as electrode materials for supercapacitor devices, microbial fuel cells with lithium ion, gas sensing of hydrogen sulfide as well as photocatalytic reduction of methyl orange dye ethanol, and nitrogen dioxide [6–9].

Indeed, many routes have been employed for the synthesis of CuO and NiO nanostructures [4–9], but in most, the crystals tend to grow into large or irregular particles. To overcome this problem and control the growth, organic surfactants are used [10,11]. Using organic surfactants is not environmentally friendly and increases the cost beside the problem of the phase purity control of the final product. Production of CuO and NiO nanostructures by thermal decomposition of organometallic molecular precursors can be considered as one of the most convenient techniques because it is not only provides a good control over purity, composition, homogeneity, phase and microstructure of the resultant products but enables us to avoid complicated synthesis procedures and conditions as well as special instruments. In the last few years, our group has been interested in the synthesis of metal, metal oxide and magnetic nanostructures, using organometallic precursors [16–20]. At the moment, our major interest is to develop inorganic or organometallic compounds for producing various metal oxide nanostructures using thermal decomposition method. Using novel compounds is the gateway for preparing nanosized materials with desired physical properties due to the associated change in the shape, size, size distribution and crystallinity.

In this work, we report a cost-efficient and simple strategy to fabricate CuO (average diameter = 17.3 nm) and NiO (average diameter = 62.4 nm) NPs via thermal decomposition of [Cu($C_{32}H_{22}N_4O_2$)]. $^3/_2$ H_2O and [Ni($C_{16}H_{11}N_3O_4$)].$2H_2O$ complexes, respectively. The study describes an experimental approach to develop our understanding of the electrical transport as well as the magnetic properties of the synthesized CuO and NiO NPs. Indeed, the electrical conduction of CuO and NiO nanostructures has been studied extensively over the last decades to predict and control their performance in the electronic devices [5,21,22]. However, there is a consensus of

* Corresponding author.
E-mail address: e.ibrahim@science.sohag.edu.eg (E.M.M. Ibrahim).

https://doi.org/10.1016/j.materresbull.2018.08.020
Received 1 February 2018; Received in revised form 7 August 2018; Accepted 14 August 2018
Available online 18 August 2018
0025-5408/

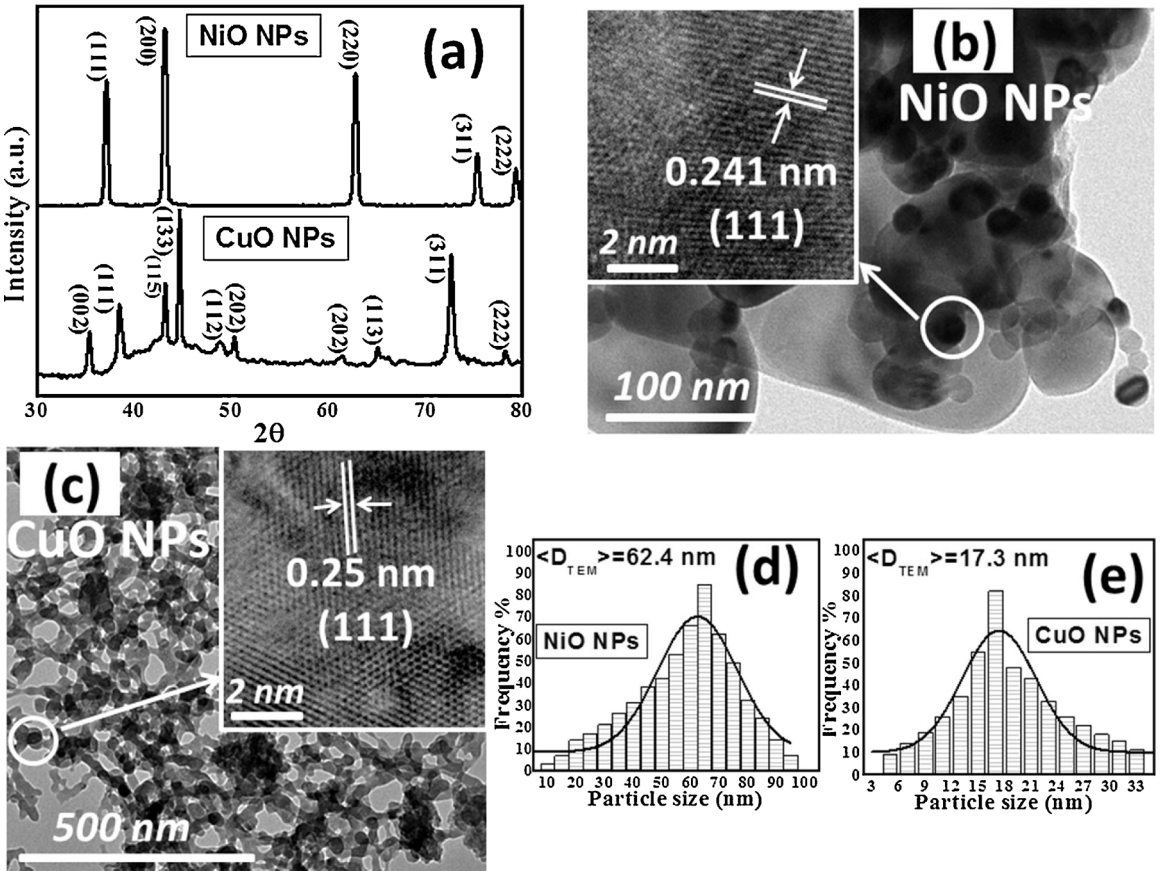

Fig. 1. a) XRD patterns; b) and c) HRTEM images (the insets show the lattice fringes); d) and e) histograms represent the size distribution of the synthesized CuO and NiO NPs, respectively.

opinion on whether the conduction is intrinsic or due to defects and on how mobile the charge carriers are. Furthermore, as the size of the particles reduces into nanometric scale both oxides exhibit changes in their electrical and magnetic properties which need further studies and investigations.

2. Experimental

2.1. Synthesis of Schiff base ligand

A tridentate imine ligand was synthesized by the condensation of an equimolar ratio of 2-hydroxy-1-napthaldehyde (5 mmol, 0.86 g) with 2-aminopyridine (5 mmol, 0.47 g) in ethanol. The resulting mixtures were refluxed for 1 h at 70 °C. After that, the solutions were gradually evaporated to a quarter of its original volume and then left to cool. The obtained orange crystals of the Schiff base ligand were filtered and then washed with ethanol several times and dried under a reduced pressure in a desiccator. Note that the purity of the compounds was tested by TLC silica gel. The full characterization data of the synthesized imine ligand are available in our previous work [23]

2.2. Synthesis of Ni- and Cu-Schiff base complexes

Ni- and Cu- Schiff base complexes ($[Cu(C_{32}H_{22}N_4O_2)].\ ^3/_2\ H_2O$ and $[Ni(C_{16}H_{11}N_3O_4)].2H_2O$) were obtained by mixing an ethanolic solution of the prepared Schiff base ligand (6 mmol, 1.49 g) with an aqueous ethanolic solution of $Cu(CH_3COO)_2.H_2O$ (3 mmol, 0.6 g) and $Ni(NO_3)_2.6H_2O$ (6 mmol, 1.74 g), respectively. The resulting mixtures were stirred magnetically for 3 h. The obtained products were evaporated overnight. The formed solid products were filtered, washed with ethanol and then dried in a vacuum chamber over anhydrous $CaCl_2$. The full characterization data of the imine ligands are available in our previous work [23,24]

2.3. Synthesis and characterization of CuO and NiO NPs

To synthesize CuO and NiO NPs, the prepared Cu- and Ni-Schiff base complexes were charged into silica crucibles and heated in air at 500 °C for 1.5 h with a heating rate of 10 °C/min. Washing with ethanol was performed for at least five times for the final products, followed by air drying at room temperature to remove any impurities. By using this facile method, metal oxide NPs could be obtained without expensive and toxic solvents or complicated equipment [25].

The morphology of the prepared NPs was investigated using JEOL high resolution transmission electron microscope (HRTEM) model JEM-2100 F at an accelerating voltage of 200 kV. PANalytical x-ray diffraction (XRD) instrument (model: PANalytical X'Pert PRO MPD) was employed for studying the structure of the sample using graphite-monochromatized Cu-K_α radiation ($\lambda = 1.54184$ Å). The instrumental resolution was determined using LaB6 standard reference material (SRM 660a) provided by National Institute of Standards and Technology (NIST), which is commonly used for calibrating line position and line shape in powder diffractometers. Rietveld refinement of the structure was performed on the XRD patterns by Maud software. The electrical conductivity was measured as a function of temperature using the two-probe method in the temperature range 300-593 K. The variation of the Seebeck coefficient with temperature was determined in order to study the thermoelectric properties of the samples. The measurements were carried out within a temperature range 83-323 K using a specially made sample holder. The electrical conductivity and Seebeck coefficient measurements were carried out in a vacuum of 10^{-3} mmHg which was found to contribute much to the thermal

stability during the measurements. The temperature of the sample and the temperature gradient in the thermoelectric measurement were sensed by standard copper-constantan thermocouples. The DC magnetic properties of the samples were studied by means of a vibrating sample magnetometer (VSM 9600-LDJ) with 1 T magnet. The AC magnetic measurements were carried out through measuring the variation of the AC susceptibility with the temperature in the temperature range 93-400 K using the Bartington Instrument MS2C system where the equipment was located in a place away from the potential sources to avoid the electrical noise. We must also take into considerations that a type S thermocouple was connected to measure the temperature and the powder sample was fixed in ceramic cylindrical pillboxes.

3. Results and discussion

Fig. 1a shows the x-ray patterns of the CuO and NiO NPs. The phase purity of the synthesized materials is obvious. The results reveal that the CuO NPs are crystallized in monoclinic structure with lattice parameters a = 4.68 Å, b = 3.43 Å, c = 5.13 Å and and β = 99.47° that match well with those reported in the JCPDS card No.: 05-0661. The diffraction peaks of NiO NPs are perfectly indexed to the face centered cubic structure with lattice parameter of a = 4.18 Å, Z = 4 and space group Fm3m in accordance to the JCPDS card file No.: 4-835. No diffraction peaks correspond to impurities or other Cu or Ni based compounds were observed. These results confirm that at 500 °C, the [Cu($C_{32}H_{22}N_4O_2$)]. $^3/_2$ H_2O and [Ni($C_{16}H_{11}N_3O_4$)].2H_2O complexes decompose completely into their corresponding metal oxides. The average crystallite size was estimated by applying the Scherrer equation $D_{XRD} = 0.89\lambda/\beta Cos(\theta)$ (β is the angular line width at half maximum intensity and θ is the Bragg's angle of the actual peak) to the most intense peak on the pattern. The D_{XRD} values were found to be ~16 and 42 nm for CuO and NiO NPs, respectively.

Fig. 1b) and c) show the HRTEM images of the NiO and CuO samples. The images illustrate that the samples consist of nearly spherical NPs. The NiO NPs seem more agglomerated which may be attributed to a weak magnetic interaction. The morphology of the NPs was highlighted by the HRTEM images depicted as insets in Fig. 1b) and c). The clear lattice fringes (marked on the inset images by white short parallel lines) indicate the high crystallinity of the NiO and CuO NPs. For pure CuO, the lattice spacing is 0.25 nm and corresponds to the (111) plane of monoclinic CuO. For NiO, the lattice fringes have a lattice spacing 0.241 nm which matches well with (111) plane of the face centered cubic structure of the NiO crystal planes [26]. Furthermore, the HRTEM data were used to extract and analyze the size and size distribution of the NPs. The corresponding histograms are depicted in Fig. 1 (d, e). The size distribution of NiO ranges from 10 to 95 nm, with an average value D_{TEM} 62 ± 1 nm, while the respective histogram of the CuO NPs implies a narrower size distribution ranging from 5 to 33 nm with average size amounts to D_{TEM} = 17 ± 0.4 nm.

The electrical conductivity (σ) was measured as a function of temperature (T). Ohmic contacts with the NPs were made using a silver paste. The I–V plots (not involved here) of the samples are linear, i.e. the derivative ∂V/∂I (or the electrical resistance) is constant proving that the contacts are ohmic and also indicating to a negligible value of the contact resistance. Experimentally, it has been observed that the conductivity of the NiO and CuO NPs increases with the increase in temperature showing a semiconductor behavior (see Fig. 2a). Several models were suggested to describe the conduction mechanisms in the metal oxides. According to the solid-state theory of semiconductors [21,27], the conduction in a semiconductor with one or more impurity levels can be described by the following formula:

$$\sigma(T) = \sigma_o e^{\frac{-E_g}{2k_B T}} + \sum_{i=1}^{n} \sigma'_{0,i} e^{\frac{-\Delta E_i}{KT}} \quad (1)$$

where, σ_o and $\sigma'_{0,i}$ are constants, E_g and ΔE_i are the band gap energy and the impurity level ionization energies and k is the Boltzmann constant.

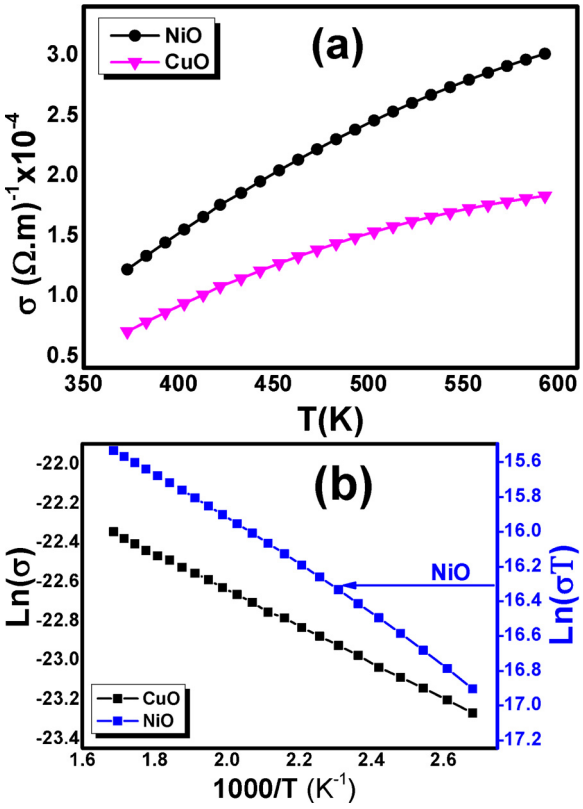

Fig. 2. a) σ vs. T b) Ln(σT) vs.1000/T for NiO and CuO NPs.

It is well known that, at low temperatures, the conduction in semiconductors is caused by the charge carriers generated by ionization of impurity levels (extrinsic conduction), and thus it is governed by the second term in Eq. (1). On the other hand, at relatively higher temperatures, the band-to-band transition mechanism dominates and in such case, the first term of Eq. 1 prevails (intrinsic conduction). In case of our CuO NPs, the σ-T plot is well represented by Eq. 1 indicating that the conduction is thermally activated type. This can be also confirmed from the corresponding Ln(σ) vs. 1000/T plot presented in Fig. 2b which shows a linear behavior. The appearance of the Ln(σ) vs. 1000/T plot in a one linear region over the whole temperature range of measurement confirms that the conduction is governed by one of the above mentioned conduction mechanisms. F. Bayansal et al. [5,21] measured the electrical dependence on temperature of CuO nanoplates based thin films deposited on glass, Cu foil, quartz and silicon substrates over a temperature range of 300-500 K. The respective Ln(ρ) vs. 1000/T plots of whether the as-synthesized thin films or those annealed at 300 °C appeared in two linear regions in the low (≤470 K) and high (≥470 K) temperature ranges. Consequently, the results of their studies reveal that the conduction mechanism transforms from impurity level ionization type to band-to-band type with the increase in temperature. For our CuO NPs, the *σ-T* plot fit well with the first term (intrinsic conduction) of Eq.1 and the energy gap E_g can be easily written as:

$$E_g = -2\frac{dLn(\sigma(T))}{d(1/T)} \quad (2)$$

E_g value of 1.5 eV was calculated from the slope of Ln(σ) vs. 1000/T plot (Eq. 2). This value is near those obtained by F. Bayansal et al. [5,21] for the CuO nanoplates in the intrinsic conduction mechanism range. The disappearance of the extrinsic conduction mechanism in our CuO NPs can be attributed to the low content of impurities which depends on the synthesis technique, particles shape and morphology.

The σ-T plot of the NiO NPs depicted in Fig. 2a exhibits also typical semiconductor features where the conductivity increases as the

temperature increases. However, the σ-T relation fit well with the following relation (Eq. 3) [28]:

$$\sigma T = \sigma_0 e^{\frac{-E_g}{k_B T}} \quad (3)$$

where, the conduction in NiO is a band-like type because of the dominance of the large polarons in the 2p band of O^{2-}. This behavior coincides well with many results reported in other literature [22,29] where it was confirmed that the conduction in nickel oxide arises from two conduction mechanisms: the small polarons in the 3d of Ni^{2+} and the large polarons in the 2 P band of O^{2-}. It has been reported that, the small polarons conduct only by means of the thermally activated hopping at temperatures above 100 K while a band like conduction due to the large polarons in the 2 P band of O^{2-} dominates at temperature higher than 200 K [30]. The linear behavior of the Ln(σT) vs. 1000/T plot illustrated in Fig. 2b confirms the large polaron conduction mechanism in the NiO NPs. The corresponding activation energy E_g was determined to be 0.116 eV. This value is comparable with the values reported in other works [22,29].

Thermoelectric power study can provide essential information about the transport properties of the materials which may not be obtained from the electrical measurements particularly in the case of low conductive materials. Variation of the Seebeck coefficient (S) with temperature (T) of the NiO and CuO NPs at hands was determined over a temperature range 83-323 K and the results are depicted in Fig. 3. Generally, S values over the whole temperature range of measurement are positive, indicating that the materials are p-type semiconductors. Besides, the increase of the Seebeck coefficient with the increase in temperature indicates that the NPs are degenerate semiconductor. For degenerate semiconductor the Seebeck coefficient can be described by the following formula assuming that the material is a quasi-free electron system [21,31].

$$S = \frac{\pi^2 k_B^2 T}{3eE_f} \quad (4)$$

where E_f and e are the Fermi energy and electron charge, respectively. The E_f value was calculated to be 0.062 and 0.07 eV for NiO and CuO NPs, respectively. The values are comparable to the value of the thermal energy $2k_BT$ at room temperature confirming the degeneracy features of the NPs. The room temperature Seebeck coefficient of our CuO and NiO NPs are equal to 89.9 and 12.1 mV/K, respectively. It is important to refer that, CuO has been previously reported as a high potential material for the thermoelectric applications [22,32,33]. The room temperature Seebeck coefficient of our CuO NPs is one order of magnitude higher than the values ~0.5 and 1.002 mV/K reported for the CuO thin film (of thickness = 612 nm) synthesized by Muhibbullah et al. [34] and N doped CuO thin film (of thickness = 920 nm) synthesized by Mondarte et al. [33], respectively. It is noteworthy that a simplified expression power factor (PF = $S^2\sigma$), is usually used for evaluating the thermoelectric efficiency of materials [35]. The PF of the

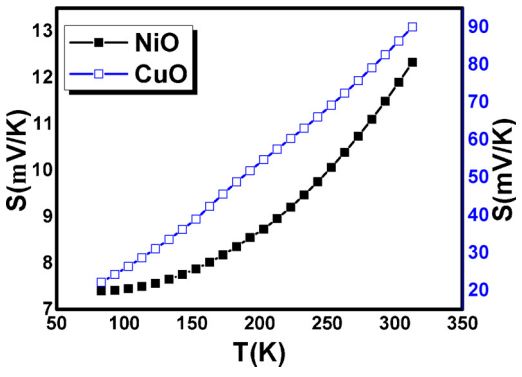

Fig. 3. Seebeck coefficient vs. temperature of the NiO and CuO NPs'.

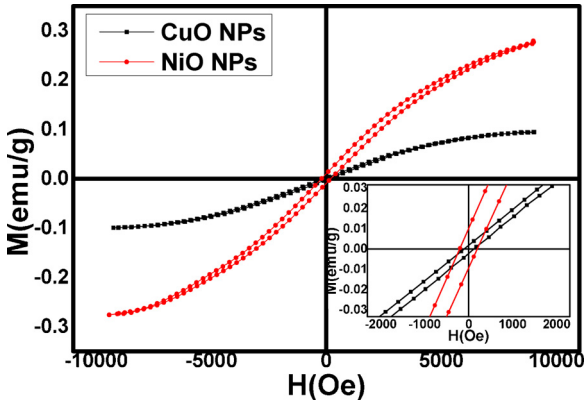

Fig. 4. M vs. H plots of the CuO and NiO NPs.

NiO and CuO NPs under study was determined to be 0.18 and 0.55 μW/mK^2. The PF value of the CuO NPs is two orders of magnitude less than that reported for the bulk material or thin films CuO [33]. The low PF value can be attributed to the low electrical conductivity resulted from the nanosized dimensions due to the associated increase of the boundaries that resist the transport of the charge carriers [33].

In bulk nickel and copper oxides, antiferromagnetic (AFM) ordering exists as a result of a super-exchange interaction between Ni^{2+} and Cu^{2+} ions, respectively mediated by O^{2-} ions [36–38]. The AFM ordering means that the magnetic moment per particle is zero due to the complete spin compensation. The (M–H) loops depicted in Fig. 4 show that the NiO and CuO NPs have small hysteresis areas indicating an existence of a weak ferromagnetic (FM) ordering. In nanosized scale, the weak FM features can be attributed mainly to the breaking of a large number of exchange bonds of the surface atoms which induces uncompensated magnetic moments in the NPs [36–38]. The native defects, such as the oxygen vacancies, can also arise magnetic ordering in oxide based semiconductors [39]. Indeed, ferromagnetic-like behavior below the bulk Néel transition temperature of CuO and NiO NPs was observed by many other researchers [36–39]. Furthermore, the FM behavior at room temperature was also observed for other nonmagnetic metallic and oxide based materials such as CdSe, In_2O_3, CeO_2, ZnO, Al_2O_3 and SnO_2 [40–42] when their dimensions were reduced to the nanoscale. Besides, Vikraman et al. [39] reported an enhancement in the FM ordering for various CuO nanostructures synthesized by chemical strategy as the particle size decreases. For our samples, the M versus H curves don't exhibit a saturation up to an applied magnetic field 10000 Oe due to the nano-metric size of the synthesized materials [43]. The magnetization at 10000 Oe (M_{10000}) and coercivity (H_c) are both estimated to be 0.1 emu/g and 109 Oe for the CuO NPs and 0.27 emu/g and 196 Oe for the NiO NPs, respectively. The conclusion that can be derived from our results is that surface modification can significantly alter the magnetic features of materials as a result of the change in the electronic structure of the nanosized materials. As the crystallite size decreases to nanometer dimensions the surface to volume ratio increases and consequently the role of the surface in the magnetic behavior becomes increasingly effective.

The Ac susceptibility was measured as a function of temperature to study the dynamic behavior of the magnetization in the samples. The measurements were carried out at a frequency of 0.3 KHz and magnetic field 250μT in a temperature range 90-405 K. In Fig. 5, the in-phase component χ' versus temperature plot of each sample exhibits a peak at a certain temperature value where it increases with the increase of temperature up to a certain value T_N and then decreases showing an antiferromagnetic-paramagnetic transition. An estimate of the Néel temperature T_N was made from the derivative of the χ'-T plots to be 188 and 150 K for CuO and NiO NPs, respectively which are less than those of the bulk materials. A decrease in the T_N value has been observed in the NPs of different antiferromagnetic materials and is attributed to the

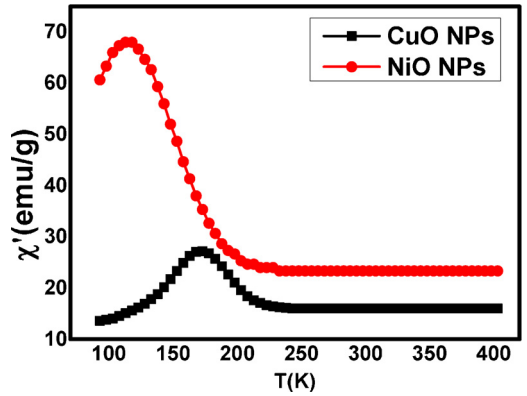

Fig. 5. χ' vs. T plots of CuO and NiO NPs.

weak exchange interactions due to the finite size effect [22,29–38]. For further explanation, the dynamic behavior in nano-sized structure can be classified into two types. The first type originates from the broad distribution of the relaxation times and results from the anisotropy energy barriers. This type dominates in the non-interacting particles where the relaxation of the magnetic moments is affected mainly by the particle energy barrier that depends on the magnetic anisotropy which in turn depends on the particle size. The second dynamic behavior type becomes significantly effective in the dense magnetic NPs systems where magnetic moments frustration occurs due to the dipolar interactions between the particles [44,45]. The dipolar interactions significantly affect the magnetic properties of the NPs particularly those of high magnetic moment μ_p. Magnetic moment μ_p values of the samples were determined using the following relation [46,47]:

$$\mu_p = 2.83\sqrt{\chi'_M T} \quad (5)$$

where, T is the temperature and χ'_M is the molar magnetic susceptibility. For our NiO and CuO NPs the calculations yield $\mu_p \approx 2000$ and 1500 μ_B, respectively. To our knowledge these values are among the highest values reported in the literature for the nanosized metal oxides [48,49] and indicate that the dipolar interaction predominates in the NPs and give a reason to the drop of the T_N values in comparison to the Néel temperatures 537 and 240 K for bulk NiO and CuO, respectively.

4. Conclusion

Thermal decomposition of $[Cu(C_{32}H_{22}N_4O_2)]$. $^3/_2$ H_2O and $[Ni(C_{16}H_{11}N_3O_4)].2H_2O$ Schiff base complexes provides a convenient, facile and effective pathway to fabricate CuO and NiO NPs. XRD and HRTEM analysis confirmed that CuO and NiO NPs with average particle size about 17 ± 0.4 and 62 ± 1 nm are uniformly formed in polycrystalline monoclinic and cubic structures, respectively, without any observed impurity phases. The synthesized CuO NPs show intrinsic conductions while NiO NPs exhibit band-like conduction with domination of the large polaron hopping mechanism. The thermoelectric measurement results show that the NPs are degenerate p-type semiconductor and the CuO NPs have high Seebeck coefficient values in comparison to those reported in previously other works and thus they are promising candidate for using in thermoelectric power generation. The CuO and NiO NPs synthesized by this novel method show weak ferromagnetic ordering which is caused by the large uncompensated magnetic spins on the nanoparticle surface. The dynamic behavior of the magnetization indicates to high dipolar interactions between the NPs.

References

[1] Mahmoud Abd El Aleem, Ali Ali El-Remaily, Ahmed M. Abu-Dief, Tetrahedron 71 (2015) 2579–2584.
[2] A.M. Abu-Dief, I.F. Nassar, W.H. Elsayed, Appl. Organometal. Chem. 30 (2016) 917–923.
[3] Ahmed M. Abu-Dief, W.S. Mohamed, Mater. Res. Express 4 (2017) 035039.
[4] W. Jia, E. Reitz, P. Shimpi, E.G. Rodriguez, P.X. Gao, Y. Lei, Mater. Res. Bull. 44 (2009) 1681.
[5] F. Bayansal, S. Kahraman, G. Çankaya, H.A. Çetinkara, H.S. Güder, H.M. çakmak, Journal of Alloys and Compounds 509 (2011) 2094–2098.
[6] A. Xiao, S. Zhou, C. Zuo, Y. Zhuan, X. Ding, Mater. Res. Bull. 70 (2015) 200–203.
[7] V. Senthilkumar, F.B. Kadumudi, N.T. Ho, J.-W. Kim, S. Park, et al., J. Power Sources 303 (2016) 363–371.
[8] Laila H. Abdel Rahman, M. Abu-Dief Ahmed, M. El-Khatib Rafat, Shimaa Mahdy Abdel-Fatah|, A.M. Adam, E.M.M. Ibrahim, Appl Organometal Chem. 32 (3) (2018) e4174.
[9] Y. Du, W. Wang, X. Li, J. Zhao, J. Ma, et al., Mater. Lett. 68 (2012) 168–170.
[10] Guanhua Lin, Wensheng Lub, Wenjie Dong, Cryst. Eng. Comm. 15 (2013) 6690–6694.
[11] K. Giannousi, G. Sarafidis, S. Mourdikoudis, A. Pantazaki, C. Dendrinou-Samara, Inorg. Chem. 53 (2014) 9657–9666.
[12] M.A. Awad, A.M. Ahmed, V.O. Khavrus, E.M.M. Ibrahim, Ceramics International 41 (2015) 10116.
[13] S.A. Saleh, S.A. Ahmed, E.M.M. Elsheikh, Journal of Superconductivity and Novel Magnetism 21 (2008) 187.
[14] S.A. Saleh, S.M. Khalil, E.M.M. Ibrahim, Superconductor Science and Technology 20 (2007) 372.
[15] M.A. Awad, E.M.M. Ibrahim, A.M. Ahmed, Journal of Thermal Analysis and Calorimetry 117 (2014) 635.
[16] E.M.M. Ibrahim, Silke Hampel, Raghunandan Kamsanipally, Juergen Thomas, Kati Erdmann, Susanne Fuessel, Christine Taeschner, Vyacheslav O. Khavrus, Thomas Gemming, Albrecht Leonhardt, Bernd Buechner, Carbon 63 (2013) 358–366.
[17] Tony Jaumann, E.M.M. Ibrahim, Silke Hampel, Diana Maier, Albrecht Leonhardt, Bernd Büchner, Chemical Vapour Deposition 17 (2013) 1–7.
[18] E.M.M. Ibrahim, Silke Hampel, A.U.B. Wolter, M. Kath, A.A. El-Gendy, R. Klingeler, Christine Täschner, Vyacheslav O. Khavrus, Thomas Gemming, Albrecht Leonhardt, Bernd Büchner, J. Phys. Chem. C 116 (2012) 22509.
[19] E.M.M. Ibrahim, Silke Hampel, Jürgen Thomas, Diana Haase, A.U.B. Wolter, Vyacheslav O. Khavrus, Christine Täschner, Albrecht Leonhardt, Bernd Büchner, J Nanopart. Res. 14 (2012) 1118.
[20] O. Vyacheslav, E.M.M. Khavrus, Alicja Ibrahim, Mark H. Bachmatiuk, A.U.B. Rümmeli, Silke Wolter, Albrecht Hampel, Leonhardt, J Nanopart. Res. 14 (2012) 914.
[21] F. Bayansal, H.A. Çetinkara, S. Kahraman, H.M. C¸ akmak, H.S. Güder, Ceramics International 38 (2012) 1859–1866.
[22] E.M.M. Ibrahim, Ahmed M. Abu-Dief, A. Elshafaie, A.M. Ahmed, Materials Chemistry and Physics 192 (2017) 41–47.
[23] H. Laila, Ahmed M. Abdel-Rahman, Emad F. Abu-Dief, Samar Newair, Kamel Hamdan, J. Photochem. & Photobiol. B: Biology 160 (2016) 18–31.
[24] Laila H. Abdel-Rahman, Ahmed M. Abu-Dief, Mohamed Shaker S. Adam, Samar Kamel Hamdan, Catal Lett 146 (2016) 1373–1396.
[25] E.M.M. Ibrahim, Laila H. Abdel-Rahman, Ahmed M. Abu-Dief, A. Elshafaie, Samar Kamel Hamdan, A.M. Ahmed, Materials Research Bulletin 99 (2018) 103–108.
[26] Shuai Wang, Da Huang, Shusheng Xu, Wenkai Jiang, Tao Wang, Jing Hu, Hu Nantao, Su Yanjie, Yafei Zhang, Zhi Yang, Phys. Chem. Chem. Phys 19 (2017) 19043–19049.
[27] B. Pejova, A. Tanusevski, I. Grozdanov, J. Solid State Chem. 178 (2005) 1786.
[28] S.A. Ahmed, E.M.M. Ibrahim, S.A. Saleh, Appl. Phys. A 85 (2006) 177.
[29] S.A. Makhlouf, M.A. Kassem, M.A. Abdel-Rahim, J. Mater. Sci. 44 (2009) 3438–3444.
[30] D. Adler, J. Feinleib, Phys. Rev. 112 (1970) 2–3.
[31] R.S. Toth, R. Kilkson, D. Trivich Phys. Rev. 122 (1961) 482.
[32] S. Dalola, G. Faglia, E. Comini, M. Ferroni, C. Soldano, D. Zappa, G. Sberveglieri, Procedia Eng. 47 (2012) 346–349.
[33] E.A. Modarate, V. Copa, A. Tuico, C.J. Vergara, E. Estacio, A. Salvador, A. Somintac, Mater. Sci. Semicond. Process. 45 (2016) 27–31.
[34] M. Muhibbullah, M.O. Hakim, M.G.M. Choudhury, Thin Solid Films 423 (2003) 103–107.
[35] M.M. Ibrahim, E.M.M. Ibrahim, S.A. Saleh, A.M.A. Hakeem, J. Alloys Compd. 429 (2007) 19–24.
[36] T.I. Arbuzova, I.B. Smolyak, A.A. Samokhvalov, S.V. Naumov, J. Exp. Theor. Phys. 86 (1998) 559.
[37] Dan Liu, Dongsheng Li, Deren Yang, AIP Advances 7 (2017) 015028.
[38] B.G. Ganga, Manoj Raama Varma, P.N. Santhosh, Cryst. Eng. Comm. 17 (2015) 7086–7093.
[39] Dhanasekaran Vikraman, Hui Joon Park, Seong-Il Kim, Mahalingam Thaiyan, Journal of Alloys and Compounds 686 (2016) 616–627.
[40] S. Tiwari, K. Rajeev, Signatures of spin-glass freezing in NiO nanoparticles, Phys. Rev. B 72 (2005) 104433.
[41] A. Sundaresan, R. Bhargavi, N. Rangarajan, U. Siddesh, C. Rao, Phys. Rev. B 74 (2006) 161306.
[42] A.A. Othman, M.A. Osman, E.M.M. Ibrahim, Manar A. Ali, A.G. Abd-Elrahim, Materials Science and Engineering B 219 (2017) 1–9.
[43] E.M.M. Ibrahim, Journal of Applied Physics 113 (2013) 154301.
[44] K. Karthik, G.K. Selvan, M. Kanagaraj, S. Arumugam, N.V. Jaya, J. Alloys Compd. 509 (2011) 181–184.
[45] A.M. Ahmed, G. Papavassiliou, H.F. Mohamed, E.M.M. Ibrahim, Journal of

Magnetism and Magnetic Materials 392 (2015) 27–41.
[46] L.H. Abdel-Rahman, R.M. El-Khatib, L.A.E. Nassr, Ahmed M. Abu-Dief, Fakhr El-Din. Lashin, Spectrochim. Acta Part A 111 (2013) 266–276.
[47] Laila H. Abdel-Rahman, Ahmed M. Abu-Dief, Mohammed Ismael, Mounir A.A. Mohamed, Ali Nahla, Hashem, Journal of Molecular Structure 1103 (2016) 232–244.
[48] Ali Ghasemi, J Clust. Sci. 27 (2016) 979–992.
[49] Marin Tadić, Matjaž Panjan, Dragana Marković, Materials Letters 64 (2010) 2129–2131.